Estimation of electrochemical and electrothermal coupling effects on self-potential data obtained during Hydraulic Fracturing in the Äspö Hard Rock Laboratory, Sweden

Nadine Haaf[1], Luis Guarracino[3], Damien Jougnot[4], Eva Schill[1,2]

[1]Karlsruhe Institute of Technology, Institute for Nuclear Waste Disposal, Hermann-von-Helmholtz-Platz 1, 76344 Eggenstein-Leopoldshafen, Germany

[2]Technical University of Darmstadt, Institute of Applied Geoscience, Schnittspahnstraße 9, 64287 Darmstadt, Germany

[3]Sorbonne Université, CNRS, EPHE, UMR 7619 METIS, 75005 Paris, France

[4]Facultad de Ciencias Astronómicas y Geofísicas, Consejo Nacional de Investigaciones Científicas y Técnicas, Universidad Nacional de La Plata, La Plata, Argentina

E-Mail: Nadine.Haaf@kit.edu

Keywords: self-potential, hydraulic fracturing, monitoring, fractured

ABSTRACT

In order to develop strategies for the mitigation of induced seismicity in enhanced geothermal systems (EGS), two out of six hydraulic fracturing experiments carried out the Äspö Hard Rock Laboratory (Sweden) in 2017 in a depth of 410 m were investigated in detail. Here we present electric self-potential monitoring during the conventional and the step-wise cyclic injection experiments HF2 and HF3. Electric self-potential data were acquired through two sensor arrays, each including nine measuring probes and one base probe, that were installed at the 410 m and 280 m levels. The experimental borehole F1 is drilled in the direction of S_{hmin}, perpendicular to the expected fracture plane. The self-potential sensors are installed sub-parallel to S_{hmin} at level 410 at a distance of 50-75 m to the borehole F1 and sub-perpendicular to S_{hmin} at level 280 m at a distance of 150-200 m to F1. The self-potential data were measured at a sampling rate of 1 Hz. SP signals were compared with hydraulic, acoustic (AE), and tilt data obtained during HF2 and HF3. Several studies of SP during injection experiments have shown that SP data are commonly interpreted as streaming potential only. Here we present two short modeling studies to additionally estimate the effect of electrochemical and electrothermal potentials on the SP amplitudes.

1. INTRODUCTION

The self-potential is used, among other things, to monitor fluid flow in the subsurface through pores and fractures. The electrokinetic potential generated by the water flow and the electric double layer (EDL) present at the solid-liquid interface are the main contributors to the SP signal during injection experiments. The basic model of the EDL consists of a zone closest to the solid phase, where the liquid charge is bound to the mineral surface, and a zone of mobile charge, the diffusion layer, which becomes neutral as it increases its distance from the solid surface. During an injection experiment, when water is injected at high pressure, this charge is carried along with the moving water, creating a charge imbalance and thus an electrical potential, usually referred to as the streaming potential. This effect has been demonstrated in previous experiments from laboratory to reservoir scale, such as the injection at Soultz-sous-Forrêts, or in laboratory experiments by Hu et al; Moore and Glaser (2020; 2007).

In addition, other coupling effects including electrochemical (e.g., Leinov and Jackson; Rembert et al. (2014; 2022)), or electrothermal (Darnet et al., 2004; Hu et al., 2020; Stoll et al., 1995) may also play a role in generating SP anomalies, the former occurring when there is a large salinity contrast between the injected fluid and the pore fluid, and the latter when there are large temperature differences. In this study we want to estimate the influence of electrochemical and electrothermal potentials on the SP data.

2. EXPERIMENTAL SETUP

Electric self-potential data were acquired through two sensor arrays, each including nine measuring probes and one base probe, that were installed at the 410 m and 280 m levels (see Figure 2-1). The experimental borehole F1 is drilled in the direction of S_{hmin}, perpendicular to the expected fracture plane. The self-potential sensors are installed sub-parallel to S_{hmin} at level 410 at a distance of 50-75 m to the borehole F1 and sub-perpendicular to S_{hmin} at level 280 m at a distance of 150-200 m to F1. A more detailed description can be found in Zang et al. (2017).
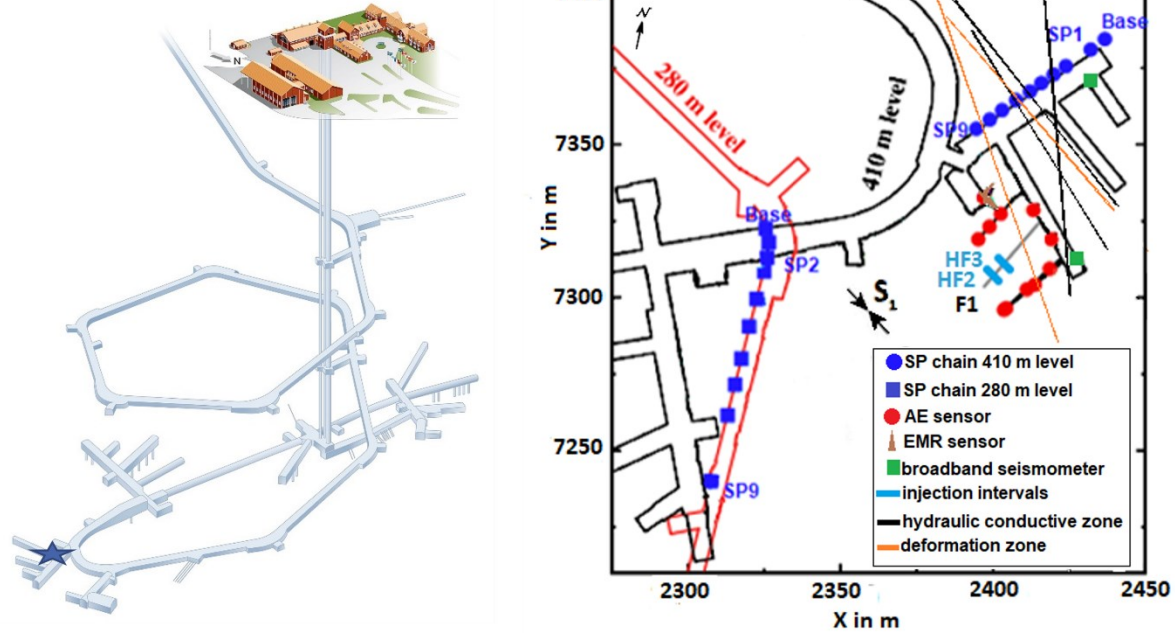
Figure 2-1: (a) The Äspö Hard Rock Laboratory and (b) the sensor array. The blue star marks the location of the experiment site. Modified after Zang et al. (2017).

3.   MODELING OF ELECTROCHEMICAL AND ELECTROTHERMAL POTENTIALS

To estimate possible influences on the streaming potential, we modeled the contribution of electrochemical and electrothermal effects on the SP amplitudes.

3.1 Electrothermal modelling

The electrothermal coupling coefficient describes the relationship between the electric potential generated and the temperature differences. The effect is calculated as

$$\Delta V_{ET} = C_{ET}\Delta T. \tag{1}$$

Corwin and Hoover (1979) estimated an average coupling between rock temperature and electric potential with $C_{ET} = 0.27 \frac{mV}{°C}$. The temperature difference was calculated using the Äspö HRL values of 16°C at 400 m depth (Stanfors et al., 1999) and the temperature of the injected tap water of 18°C. Thus, an electrothermal potential $\Delta V_{ET} = 0.5\ mV$ was estimated.

3.2   Electrochemical modelling

The following approach follows the calculation of Darnet et al; Darnet et al. (2004; 2006) and Fetter (1993). The electrochemical potential can be calculated using following equation:

$$\Delta V_{EC} = \varphi \frac{RT}{Ne}\frac{u_{CL}-u_{Na}}{u_{CL}+u_{Na}}\frac{\Delta C}{C} = C_{EC}\Delta C \tag{2}$$

Whereby the electrochemical coupling coefficient is C_{EC} and the salinity profile as ΔC. R is the molar gas constant, T the temperature of the fluid, φ is the porosity, N is Avogadro's number, e the unit charge, u the ionic mobility of Natrium and chloride, respectively, and C the electrolyte salinity.

The physical quantities are collected and defined in the following Table 1.

Table 1: Overview of quantities used for the electrochemical modeling.

Quantity	Value	Unit	Note/reference
Molar gas constant **R**	8.3144598	J mol^{-1} K^{-1}	Holleman et al. (2007)
Unit charge **e**	1.602176634x10^{-19}	C	Holleman et al. (2007)

Avogadro's number N	$6.02214076 \times 10^{23}$	Mol^{-1}	Holleman et al. (2007)
Ionic mobility u_{Na}	5.2×10^{-8}	$m^2 s^{-1} V^{-1}$	Holleman et al. (2007)
Ionic mobility u_{Cl}	7.9×10^{-8}	$m^2 s^{-1} V^{-1}$	Holleman et al. (2007)
Initial concentration of injected water C_0	0.00386	$Mol L^{-1}$	226 ppm Swedish tap water, Kaunisto et al. (2017)
Temperature	291.15	K	
Longitudinal dispersivity α_L	0.45	m	Value for crystalline rock by Mazurek et al. (2003)
Hydrodynamic longitudinal dispersion coefficient D_L	4.7735×10^{-4}	$m^2 s^{-1}$	**Error! Reference source not found.**)
Fluid velocity v_r	0.001060776627006	$m s^{-1}$	Equation (7)
Flow rate Q	5.0×10^{-5}	$m^3 s^{-1}$	Average flow rate of HF2
Molecular diffusion coefficient D^*	5.0×10^{-10}	$m^2 s^{-1}$	Fetter (1993)
Time t	5000	s	
Porosity φ	0.26	%	Widestrand et al. (2010)
Open hole section h	5.0	m	Estimated radius of largest elliptical fracture plane of AE activity during HF2 and HF3 (Niemz et al., 2020)
Average frontal position of the injected water r_0	0.5-5.0	m	Minimal (test interval) and maximal (see h) radius were tested
Concentration pore fluid C_1	3.422×10^{-5}	$Mol L^{-1}$	

To estimate the salinity profile ΔC one assumes a radial flow in a homogenous porous medium. Following Fetter (1993) we get the equation for the mass transport

$$D_L \frac{\partial^2 C}{\partial r^2} + \left(\frac{D_L}{r} - v_r\right)\frac{\partial C}{\partial r} = \frac{\partial C}{\partial t} \qquad (3)$$

where D_L is the hydrodynamic longitudinal dispersion coefficient, v_r is the average linear fluid velocity, r is the radial distance from the well, and t is time.

If we assume a continuous injection a solution for equation (2) can be found after Fetter (1993) as

$$C(r,t) = C_0 + ((C_1 - C_0)/2) erfc\left[(r - r_0)/2\sqrt{(D_L t)}\right]. \qquad (4)$$

The dispersion coefficient D_L is defined as

$$D_L = \alpha_L v_r + D^* \qquad (5)$$

where D^* is molecular diffusion coefficient and α_L is the longitudinal dispersivity. The mass conversation equation of the injected water is used to estimate the average linear fluid velocity

$$Qt = \pi r_0^2 h \varphi \qquad (6)$$

where Q is the injection rate, r_0 is the average frontal position of the injected water and h is the open hole section. Here, the fracture planes are estimated based on the hypocenter location of the acoustic emissions AEs of each cycle (Niemz et al., 2020). In particular, assuming that the fluid flows through the induced fractures, we consider the largest fracture plane (HF2 RF5) during the experiment. It has an ellipsoidal distribution and a radius of about 5 m. Thus, the maximum value of r_0 is 5 m. The minimum value of r_0 is assumed to be the

length of the test interval, 0.5 m. In addition, it is assumed that the fluid velocity, v_r, is equal to the velocity of the injected water front, v_0, and follows

$$v_r \approx v_0 = \frac{dr_0}{dt} = \frac{Q}{2\pi\varphi}\left(\frac{Qt}{\pi h\varphi}\right)^{-1/2}. \tag{7}$$

The electrochemical potentials are calculated using equations $\Delta V_{ET} = C_{ET}\Delta T$.
(1) and **Error! Reference source not found.**) over a spatial distribution of 100 m and a time window of 100 min. The fracture planes are estimated based on the hypocenter location of the acoustic emissions events of each (re)fracturing stage (Niemz et al., 2020). In particular, assuming that the fluid flows through the fractures, the largest fracture plane (HF2 RF5) is considered to have an ellipsoidal distribution and a radius of about 5 m. Thus, the maximum value of r_0 is 5 m. The minimum value of r_0 is assumed to be the length of the test interval, 0.5 m. Figure 3-1 shows the calculated amplitudes of the electrochemical potentials. The example for the minimum average frontal position of the injected water shows values from 0.22 mV to 0.76 mV, while the results for r0=5 m show a range from -0.75 mV to 0.78 mV.
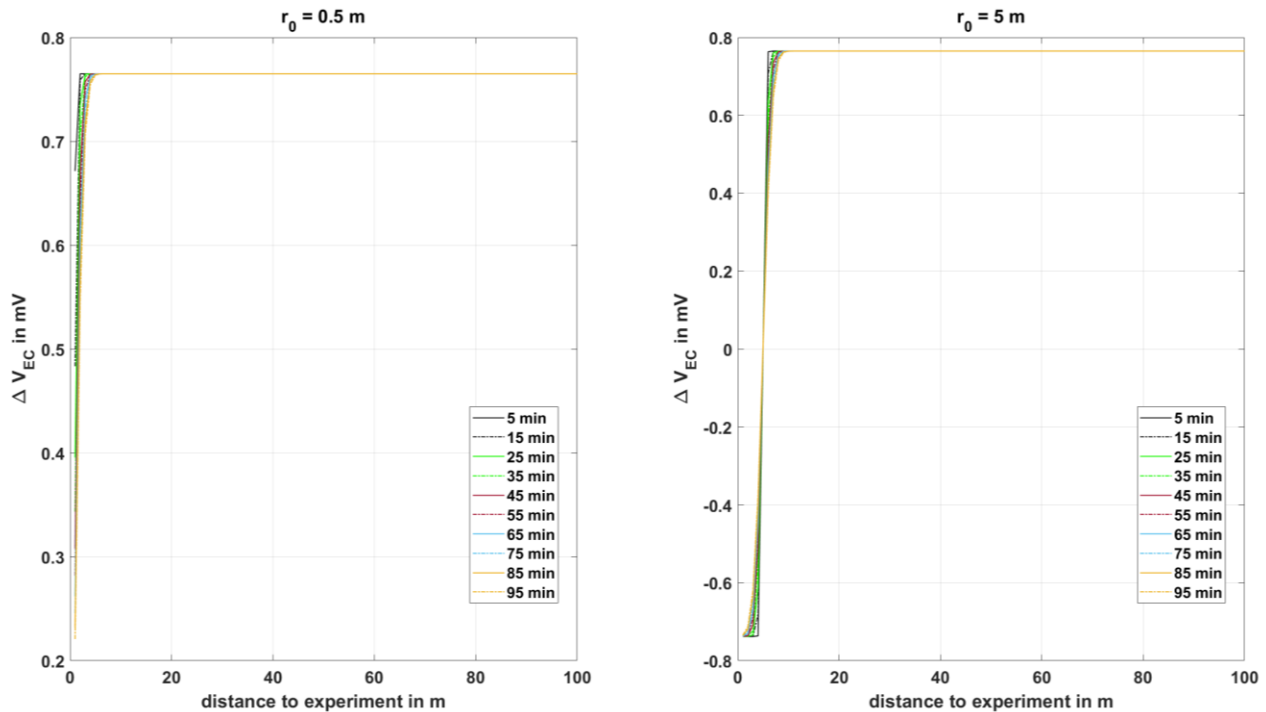

Figure 3-1: Electrochemical potentials for r_0 = 0.5 m and r_0 = 5 m. The potentials are calculated for several time steps starting by 5 and ending with 95 minutes.

4   CONCLUSION

The present study aims to contribute to the understanding of the SP amplitudes obtained during injection experiments. It is shown that in this case the SP anomalies are rarely generated by electrochemical or electrothermal coupling effects. Both effects can explain only a significant small fraction of the 100s of mV of the SP amplitudes.

REFERENCES

Corwin, R.F., Hoover, D.B., 1979. The self-potential method in geothermal exploration. GEOPHYSICS 44 (2), 226–245.

Darnet, M., Maineult, A., Marquis, G., 2004. On the origins of self-potential (SP) anomalies induced by water injections into geothermal reservoirs. Geophys. Res. Lett. 31 (19), 226.

Darnet, M., Marquis, G., Sailhac, P., 2006. Hydraulic stimulation of geothermal reservoirs: fluid flow, electric potential and microseismicity relationships. Geophys. J. Int. 166 (1), 438–444.

Fetter, C.W., 1993. Contaminant Hydrogeology. Macmillan Publishing Company, New York.

Holleman, A.F., Wiberg, E., Wiberg, N., Fischer, G., 2007. Lehrbuch der anorganischen Chemie, 102., stark umgearbeitete und verbesserte Auflage ed. De Gruyter Reference Global. Walter de Gruyter, Berlin, New York, 2149 pp.

Hu, L., Ghassemi, A., Pritchett, J., Garg, S., Ishido, T., 2020. Self-Potential Response in Laboratory Scale EGS Stimulation. Rock Mech Rock Eng 53 (2), 691–703.

Kaunisto, T., Latva, M., Engelsen, C., Kloppenborg, S., Rod, O., Gulbrandsen-Dahl, S., 2017. Nordic drinking water quality: A Nordic Innovation project. Nordic Innovation project MaiD.

Leinov, E., Jackson, M.D., 2014. Experimental measurements of the SP response to concentration and temperature gradients in sandstones with application to subsurface geophysical monitoring. JGR Solid Earth 119 (9), 6855–6876.

Mazurek, M., Jakob, A., Bossart, P., 2003. Solute transport in crystalline rocks at Aspö--I: geological basis and model calibration. Journal of contaminant hydrology 61 (1-4), 157–174.

Moore, J.R., Glaser, S.D., 2007. Self-potential observations during hydraulic fracturing. J. Geophys. Res. 112 (B2).

Niemz, P., Cesca, S., Heimann, S., Grigoli, F., von Specht, S., Hammer, C., Zang, A., Dahm, T., 2020. Full-waveform-based characterization of acoustic emission activity in a mine-scale experiment: a comparison of conventional and advanced hydraulic fracturing schemes. Geophysical Journal International 222 (1), 189–206.

Rembert, F., Jougnot, D., Luquot, L., Guérin, R., 2022. Interpreting Self-Potential Signal during Reactive Transport: Application to Calcite Dissolution and Precipitation. Water 14 (10), 1632.

Stanfors, R., Rhén, I., Tullborg, E.-L., Wikberg, P., 1999. Overview of geological and hydrogeological conditions of the Äspö hard rock laboratory site. Applied Geochemistry 14 (7), 819–834.

Stoll, J., Bigalke, J., Grabner, E.W., 1995. Electrochemical modelling of self-potential anomalies. Surv Geophys 16 (1), 107–120.

Widestrand, H., Byegård, J., Selnert, E., Skålberg, M., Höglund, S., Gustafsson, E., 2010. Long Term Sorption Diffusion Experiment (LTDE-SD) – Supporting laboratory program – Sorption diffusion experiments and rock material characterisation: With supplement of adsorption studies on intact rock samples from the Forsmark and Laxemar site investigations (SKB R-10-66).

Zang, A., Stephansson, O., Stenberg, L., Plenkers, K., Specht, S., Milkereit, C., Schill, E., Kwiatek, G., Dresen, G., Zimmermann, G., Dahm, T., Weber, M., 2017. Hydraulic fracture monitoring in hard rock at 410 m depth with an advanced fluid-injection protocol and extensive sensor array. Geophys. J. Int. 208 (2), 790–813.